

# Measurement and topological quantum criticality of local and nonlocal Chern markers

Paolo Mognini<sup>1</sup>, Bastien Lapierre<sup>2</sup>, R. Chitra<sup>3</sup>, and Wei Chen<sup>4</sup>

<sup>1</sup>T.C.M. group, Cavendish Laboratory, University of Cambridge, 19 J J Thomson Avenue, Cambridge, CB3 0HE, United Kingdom

<sup>2</sup>Department of Physics, University of Zurich, Winterthurerstrasse 190, 8057 Zurich, Switzerland

<sup>3</sup>Institute for Theoretical Physics, ETH Zurich, 8093 Zurich, Switzerland

<sup>4</sup>Department of Physics, PUC-Rio, Rio de Janeiro 22451-900, Brazil

E-mail: wchen@puc-rio.br

## Abstract.

In contrast to diverse momentum space topological invariants, the local Chern marker in two-dimensional time-reversal breaking systems is known to be a direct probe of topological order in real space. Using finite temperature linear response theory, we demonstrate that this Chern marker is equivalent to the lattice charge polarization susceptibility to a circularly polarized electric field. A Chern marker spectral function is also introduced to describe the frequency-resolved circular dichroism measurement. We find that the nonlocal charge polarization susceptibility naturally leads to the notion of a Chern correlator which provides a distinct measure of topological correlations present in the system. From the off-diagonal elements of the Chern operator, a nonlocal Chern marker is further introduced, and we show that it is equivalent to a previously introduced Wannier state correlation function, a sensitive probe of topological phase transitions. Our work thus highlights the deep connection between real space measures of topological order and topological correlations, and experimentally measurable observables.

## 1. Introduction

The topological order in two-dimensional (2D) time-reversal (TR) breaking systems has been an important subject in the research of topological materials, and also one of the earliest systems discovered to have nontrivial topological properties [1]. The topological invariant in these systems is described by the Chern number, which is usually detected experimentally via measuring the quantized Hall conductance [2] that in practice is attributed to the formation of edge states. The bulk band structure, on the other hand, shows the same gapped energy spectrum in both the topologically trivial and nontrivial phases, and therefore bulk measurements not involving edge states are often not considered feasible to identify the Chern number. However, the theoretical proposal of the Chern marker and other real space constructions changed this paradigmatic

viewpoint [3, 4, 5, 6, 7, 8, 9, 10, 11, 12]. Through expressing the Chern number in terms of the projectors into the filled and empty bands, the Chern marker is introduced as a local quantity that is well-defined everywhere in the bulk, and recovers the Chern number in the clean, thermodynamic limit. In fact, it has been shown that such a real space formalism of topological invariant is also possible in other dimensions and symmetry classes [13, 14, 15, 16, 17, 18]. It was further recognized recently that the Chern number and Chern marker are related to the circular dichroism of the 2D material [19, 20, 21, 22], and so is the Berry curvature that integrates to the Chern number [23, 24], pointing to the possibility of directly detecting the topological order by means of bulk optical measurements.

In this paper, we advance the theory of Chern markers by introducing a number of new aspects related to its measurement and topological quantum criticality. Concerning the measurement of the Chern marker, we generalize a recently proposed linear response theory of Berry curvature to real space [24], which clarifies that the Chern marker is in fact the charge polarization susceptibility of the lattice caused by circularly polarized electric field. Our theory introduces a Chern marker spectral function that characterizes the absorption rate of the electric field at a specific frequency in the circular dichroism experiment, and moreover generalizes both the Chern marker and its spectral function to nonzero temperature, which greatly improves their relevance to realistic experimental situations. In addition, the nonlocal charge polarization susceptibility is shown to represent a Chern correlator, which spatially sums to the Chern marker and hence plays the role of the internal structure of the Chern marker. The magnitude of the correlator is found to increase as the system enters topologically nontrivial phases, suggesting that it measures a kind of topological correlation in the system. Finally, we introduce a quantity to characterize the quantum criticality near topological phase transitions (TPTs) that we call nonlocal Chern marker, which is an object defined from the off-diagonal elements of the Chern operator, in contrast to the usual Chern marker defined from the diagonal element of the same operator. This nonlocal Chern marker is equivalent to a previously proposed correlation function that measures the overlap between Wannier functions localized at different home cells [25, 26, 27], and becomes long-ranged as the system approaches TPTs, owing to the diverging Berry curvature in momentum space.

## **2. Linear response theory of local Chern marker**

### *2.1. Local Chern marker in terms of Wannier states*

Our aim is to construct a linear response theory for the local real space Chern marker and connect it to experimental measurables. For this purpose, we first review the derivation of the Chern marker following the original work by Bianco and Resta [7], with an emphasis on the relation to Wannier states in the homogeneous case. We first establish our notations for the bands and Bloch states. The indices  $n$  and  $m$

denote the valence and conduction bands respectively, while  $\ell$  denotes both bands. The overlap  $\langle \mathbf{r} | u_{\ell \mathbf{k}} \rangle = u_{\ell \mathbf{k}}(\mathbf{r}) = e^{-i\mathbf{k}\cdot\mathbf{r}} \psi_{\ell \mathbf{k}}(\mathbf{r})$  denotes the periodic part of the Bloch state satisfying  $u_{\ell \mathbf{k}}(\mathbf{r}) = u_{\ell \mathbf{k}}(\mathbf{r} + \mathbf{R})$ , with  $\mathbf{R}$  a Bravais lattice vector. In the homogeneous and thermodynamic limit, the Bloch state of each band  $|u_{\ell \mathbf{k}}\rangle$  defines a Wannier state  $|\mathbf{R}\ell\rangle$  by

$$|u_{\ell \mathbf{k}}\rangle = \sum_{\mathbf{R}} e^{-i\mathbf{k}\cdot(\hat{\mathbf{r}}-\mathbf{R})} |\mathbf{R}\ell\rangle, \quad |\mathbf{R}\ell\rangle = \sum_{\mathbf{k}} e^{i\mathbf{k}\cdot(\hat{\mathbf{r}}-\mathbf{R})} |u_{\ell \mathbf{k}}\rangle, \quad (1)$$

where  $\hat{\mathbf{r}}$  is the position operator and the normalization factors are ignored for simplicity. The Wannier function at position  $\mathbf{r} = (x, y)$  is given by  $\langle \mathbf{r} | \mathbf{R}n \rangle = W_n(\mathbf{r} - \mathbf{R})$ , which localizes around the home cell  $\mathbf{R}$  in real space.

For a general model that contains  $N_-$  valence bands, the periodic part of the fully antisymmetric valence band state at momentum  $\mathbf{k}$  is given by

$$|u^{\text{val}}(\mathbf{k})\rangle = \frac{1}{\sqrt{N_-!}} \epsilon^{n_1 n_2 \dots n_{N_-}} |u_{n_1 \mathbf{k}}\rangle |u_{n_2 \mathbf{k}}\rangle \dots |u_{n_{N_-} \mathbf{k}}\rangle. \quad (2)$$

The Berry curvature of this valence band state in Eq. (2) on the  $xy$ -plane of a 2D system is given by [28]

$$\begin{aligned} \Omega_{xy}(\mathbf{k}) &= i \langle \partial_x u^{\text{val}}(\mathbf{k}) | \partial_y u^{\text{val}}(\mathbf{k}) \rangle - i \langle \partial_y u^{\text{val}}(\mathbf{k}) | \partial_x u^{\text{val}}(\mathbf{k}) \rangle \\ &= \sum_n [i \langle \partial_x u_{n\mathbf{k}} | \partial_y u_{n\mathbf{k}} \rangle - i \langle \partial_y u_{n\mathbf{k}} | \partial_x u_{n\mathbf{k}} \rangle]. \end{aligned} \quad (3)$$

Note that the Berry curvature is additive in the curvatures of each individual valence band. We rewrite the corresponding Chern number  $\mathcal{C}$  (defined as the momentum space integration of  $\Omega_{xy}(\mathbf{k})$ ) [7] as

$$\begin{aligned} \mathcal{C} &= \int \frac{d^2 \mathbf{k}}{(2\pi)^2} \Omega_{xy}(\mathbf{k}) \\ &= \sum_{n,m} \int \frac{d^2 \mathbf{k}}{(2\pi)^2} i \langle \partial_x u_{n\mathbf{k}} | u_{m\mathbf{k}} \rangle \langle u_{m\mathbf{k}} | \partial_y u_{n\mathbf{k}} \rangle - (x \leftrightarrow y) \end{aligned} \quad (4)$$

where the volume of the unit cell  $A_c = a^2 = 1$  is set to unity for simplicity. To relate the Chern number to our proposed Chern marker, we introduce the lattice position operator  $\hat{x}$  defined by

$$\hat{x} = \sum_{\mathbf{r}\sigma} |\mathbf{r}, \sigma\rangle x_{\mathbf{r}} \langle \mathbf{r}, \sigma| \equiv \sum_{\mathbf{r}} |\mathbf{r}\rangle x_{\mathbf{r}} \langle \mathbf{r}|, \quad (5)$$

where  $\sigma$  denotes the internal degrees of freedom within a unit cell like orbital, spin, sublattice, etc. In the following, we extensively use the identity linking the non-Abelian Berry connection to the charge polarization of the eigenstates and Wannier states [7, 29, 30, 31, 25, 26]

$$\begin{aligned} i \langle u_{m\mathbf{k}} | \partial_x u_{n\mathbf{k}} \rangle &= \langle \psi_{m\mathbf{k}} | \hat{x} | \psi_{n\mathbf{k}} \rangle \\ &= \sum_{\mathbf{R}} e^{i\mathbf{k}\cdot\mathbf{R}} \langle \mathbf{0}m | \hat{x} | \mathbf{R}n \rangle = \sum_{\mathbf{R}} e^{-i\mathbf{k}\cdot\mathbf{R}} \langle \mathbf{R}m | \hat{x} | \mathbf{0}n \rangle \quad \forall m \neq n. \end{aligned} \quad (6)$$

Using Eqs.(5) and (6),  $\mathcal{C}$  can be expressed in terms of the Wannier states [7]:

$$\begin{aligned}
 \mathcal{C} &= \sum_{nm} \int \frac{d^2\mathbf{k}}{(2\pi)^2} i \langle \psi_{n\mathbf{k}} | \hat{x} | \psi_{m\mathbf{k}} \rangle \langle \psi_{m\mathbf{k}} | \hat{y} | \psi_{n\mathbf{k}} \rangle - (x \leftrightarrow y) \\
 &= \sum_{nm} \int \frac{d^2\mathbf{k}}{(2\pi)^2} \int \frac{d^2\mathbf{k}'}{(2\pi)^2} i \langle \psi_{n\mathbf{k}} | \hat{x} | \psi_{m\mathbf{k}'} \rangle \langle \psi_{m\mathbf{k}'} | \hat{y} | \psi_{n\mathbf{k}} \rangle - (x \leftrightarrow y) \\
 &= \sum_{nm} \sum_{\mathbf{R}} i \langle \mathbf{0}n | \hat{x} | \mathbf{R}m \rangle \langle \mathbf{R}m | \hat{y} | \mathbf{0}n \rangle - (x \leftrightarrow y) \\
 &= \sum_{nm} \sum_{\mathbf{R}} i \int d\mathbf{r} \int d\mathbf{r}' x_{\mathbf{r}} W_n^*(\mathbf{r}) W_m(\mathbf{r} - \mathbf{R}) y_{\mathbf{r}'} W_m^*(\mathbf{r}' - \mathbf{R}) W_n(\mathbf{r}') \\
 &\quad - (x \leftrightarrow y), \tag{7}
 \end{aligned}$$

where the second line is valid because the matrix elements for  $\mathbf{k} \neq \mathbf{k}'$  vanish. In terms of the projection operators to the valence and conduction band states

$$\hat{P} = \sum_n \int \frac{d^2\mathbf{k}}{(2\pi)^2} |\psi_{n\mathbf{k}}\rangle \langle \psi_{n\mathbf{k}}|, \quad \hat{Q} = \sum_m \int \frac{d^2\mathbf{k}'}{(2\pi)^2} |\psi_{m\mathbf{k}'}\rangle \langle \psi_{m\mathbf{k}'}|, \tag{8}$$

the Chern number can be recast as

$$\mathcal{C} = i \text{Tr}_{\text{cell}} \left[ \hat{P} \hat{x} \hat{Q} \hat{y} - \hat{P} \hat{y} \hat{Q} \hat{x} \right] \equiv i \sum_{\sigma} \langle \sigma | \left[ \hat{P} \hat{x} \hat{Q} \hat{y} - \hat{P} \hat{y} \hat{Q} \hat{x} \right] | \sigma \rangle, \tag{9}$$

where  $\text{Tr}_{\text{cell}}$  denotes the trace over a unit cell. The operator  $\hat{\mathcal{C}} \equiv i[\hat{P}\hat{x}\hat{Q}\hat{y} - \hat{P}\hat{y}\hat{Q}\hat{x}]$  will be referred to as the Chern operator.

To see the explicit operator form, we consider a 2D tight-binding Hamiltonian  $H = \sum_{\mathbf{r}\mathbf{r}'\sigma\sigma'} t_{\mathbf{r}\mathbf{r}'\sigma\sigma'} c_{\mathbf{r}\sigma}^\dagger c_{\mathbf{r}'\sigma'}$  with eigenstates  $H|E_l\rangle = E_l|E_l\rangle$ . In terms of  $|E_l\rangle$ , the projectors in Eq. (8) take the form

$$\hat{P} = \sum_n |E_n\rangle \langle E_n|, \quad \hat{Q} = \sum_m |E_m\rangle \langle E_m|. \tag{10}$$

Since the eigenstate  $|E_l\rangle$  is now written in the position basis  $|\mathbf{r}, \sigma\rangle$ , one can introduce the notion of a local Chern marker at any unit cell position  $\mathbf{r}$  in terms of the position operators  $\hat{x}_{\mathbf{r}}, \hat{y}_{\mathbf{r}}$  [7]

$$\hat{x}_{\mathbf{r}} = \hat{x}_{\mathbf{r}}^\dagger = |\mathbf{r}\rangle x_{\mathbf{r}} \langle \mathbf{r}| = \sum_{\sigma} |\mathbf{r}, \sigma\rangle x_{\mathbf{r}} \langle \mathbf{r}, \sigma| = \sum_{\sigma} x_{\mathbf{r}} c_{\mathbf{r}\sigma}^\dagger c_{\mathbf{r}\sigma}. \tag{11}$$

and likewise for  $\hat{y}_{\mathbf{r}}$ . Using Eq.(11), the local Chern marker is defined by

$$\begin{aligned}
 \mathcal{C}(\mathbf{r}) &= \sum_{\sigma} \langle \mathbf{r}, \sigma | \hat{\mathcal{C}} | \mathbf{r}, \sigma \rangle \equiv i \langle \mathbf{r} | \left[ \hat{P} \hat{x} \hat{Q} \hat{y} - \hat{P} \hat{y} \hat{Q} \hat{x} \right] | \mathbf{r} \rangle \\
 &= \sum_{nm} \sum_{\mathbf{R}} i \langle \mathbf{0}n | \hat{x}_{\mathbf{r}} | \mathbf{R}m \rangle \langle \mathbf{R}m | \hat{y} | \mathbf{0}n \rangle - (x \leftrightarrow y), \tag{12}
 \end{aligned}$$

To facilitate a comparison with linear response theory in Sec. 2.3, the local Chern marker in Eq. (12) can be conveniently rewritten as

$$\begin{aligned}
 \mathcal{C}(\mathbf{r}) &= \sum_{nm} \{ i \langle \mathbf{r} | \hat{x} | E_m \rangle \langle E_m | \hat{y} | E_n \rangle \langle E_n | \mathbf{r} \rangle - (x \leftrightarrow y) \} \\
 &= \sum_{nm} \{ i \langle E_n | \hat{x}_{\mathbf{r}} | E_m \rangle \langle E_m | \hat{y} | E_n \rangle - (x \leftrightarrow y) \}. \tag{13}
 \end{aligned}$$

## 2.2. Measurement protocols of Chern number at zero temperature

We now briefly mention a measurement of the Chern number at zero temperature based on circular dichroism that has been proposed previously [19, 20, 21, 22], which will be generalized to nonzero temperature in the next section. We assume that the lattice system is subjected to a circularly polarized electric field of magnitude  $E^0$  and frequency  $\omega$ , leading to an additional term in the hamiltonian

$$H_{c_1, c_2} = (\hat{x} \pm i\hat{y})qE^0 e^{-i\omega t}, \quad (14)$$

where  $c_i$  labels the polarization and  $q$  is the charge. Fermi's Golden rule dictates that the total transition rate from all the occupied states  $|E_n\rangle$  to all the empty states  $|E_m\rangle$  is

$$\Delta\gamma^{c_1, c_2}(\omega) = \frac{2\pi}{\hbar} \sum_{nm} |\langle E_m | H_{c_1, c_2} | E_n \rangle|^2 \delta(\hbar\omega + E_n - E_m), \quad (15)$$

Using Eq. (9), we find that the Chern number  $\mathcal{C}$  is directly proportional to the frequency integration of the differential transition rates for the two polarizations, hence circular dichroism,

$$\int d\omega (\Delta\gamma^{c_1}(\omega) - \Delta\gamma^{c_2}(\omega)) = 4\pi A \left( \frac{qE^0}{\hbar} \right)^2 \mathcal{C}, \quad (16)$$

where  $A$  is the unit cell area.

## 2.3. Linear response theory of nonzero temperature Chern marker

The result linking the Chern number to the circular dichroism can be generalized to nonzero temperatures using linear response theory. Though our approach is very similar to the Kubo formula for the absorptive part of the antisymmetric optical conductivity in TR-breaking crystals [32], our primary focus is on topological features related to the Chern marker. We consider the application of a uniform electric field  $E^y$  of frequency  $\omega$  along the  $y$ -direction, causing the perturbation

$$\delta H(t) = - \sum_{\mathbf{r}} \hat{y}_{\mathbf{r}}(t) q E^y e^{-i\omega t}, \quad (17)$$

using the local operator defined in Eq. (11). Within linear response,

$$\langle \hat{x}_{\mathbf{r}}(t) \rangle_0 = -\chi_{xy}(\mathbf{r}, t) q E^y e^{-i\omega t}. \quad (18)$$

The charge polarization susceptibility  $\chi_{xy}$  at  $\mathbf{r}$  caused by an oscillating field of frequency  $\omega$  is generally nonlocal, i.e. an electric field applied at site  $\mathbf{r}'$  can cause a charge polarization at site  $\mathbf{r}$ , leading to the nonlocal charge polarization response function,

$$\chi_{xy}(\mathbf{r}, \mathbf{r}', t - t') = -i\theta(t - t') \langle \hat{x}_{\mathbf{r}}(t) \hat{y}_{\mathbf{r}'}(t') - \hat{y}_{\mathbf{r}'}(t') \hat{x}_{\mathbf{r}}(t) \rangle. \quad (19)$$

In the Lehmann representation,

$$\chi_{xy}(\mathbf{r}, \mathbf{r}', \omega) = \sum_{\ell\ell'} \langle E_{\ell} | \hat{x}_{\mathbf{r}} | E_{\ell'} \rangle \langle E_{\ell'} | \hat{y}_{\mathbf{r}'} | E_{\ell} \rangle \frac{f(E_{\ell}) - f(E_{\ell'})}{\omega + E_{\ell} - E_{\ell'} + i\eta}, \quad (20)$$

where  $\eta$  is a small artificial broadening. Here  $\ell$  and  $\ell'$  both include the filled (valence) and empty (conduction) states. The local susceptibility  $\chi_{xy}(\mathbf{r}, \omega) = \int_{\mathbf{r}'} d\mathbf{r}' \chi_{xy}(\mathbf{r}, \mathbf{r}', \omega)$  is given by

$$\chi_{xy}(\mathbf{r}, \omega) = \sum_{\ell\ell'} \langle E_\ell | \hat{x}_{\mathbf{r}} | E_{\ell'} \rangle \langle E_{\ell'} | \hat{y} | E_\ell \rangle \frac{f(E_\ell) - f(E_{\ell'})}{\omega + E_\ell - E_{\ell'} + i\eta}. \quad (21)$$

We now introduce the Chern number local spectral function at nonzero temperature defined at positive frequency  $\omega > 0$  (since we aim to define an observable purely related to absorption processes)

$$\begin{aligned} \mathcal{C}^d(\mathbf{r}, \omega) &= -\frac{1}{\pi} \text{Re} [\chi_{xy}(\mathbf{r}, \omega) - \chi_{yx}(\mathbf{r}, \omega)] \\ &= \sum_{\ell < \ell'} \text{Re} [i \langle E_\ell | \hat{x}_{\mathbf{r}} | E_{\ell'} \rangle \langle E_{\ell'} | \hat{y} | E_\ell \rangle - (x \leftrightarrow y)] \\ &\quad \times [f(E_\ell) - f(E_{\ell'})] \delta(\omega + E_\ell - E_{\ell'}). \end{aligned} \quad (22)$$

The superscript  $d$  stands for “dressed”, following the notation in the linear response theory of the interaction-dressed Berry curvature [24]. Here  $\ell < \ell'$  is a shortcut notation for  $E_\ell < E_{\ell'}$  ensuring absorption processes as  $f(E_\ell) - f(E_{\ell'}) > 0$ . A global spectral function can also be defined via  $\mathcal{C}^d(\omega) = \sum_{\mathbf{r}} \mathcal{C}^d(\mathbf{r}, \omega)$ . We now define the generalized nonzero temperature local Chern marker as

$$\mathcal{C}^d(\mathbf{r}) = \int d\omega \mathcal{C}^d(\mathbf{r}, \omega). \quad (23)$$

At zero temperature, as  $f(E_\ell) = \theta(-E_\ell)$ , Eq. (22) only picks up filled states  $n$  in the valence band and empty states  $m$  in the conduction band and  $\mathcal{C}^d(\mathbf{r})|_{T=0} = \mathcal{C}(\mathbf{r})$  recovering the local Chern marker in Eq. (13). To summarize,  $\mathcal{C}^d(\mathbf{r})$  is a real space generalization of a topological probe which is intimately related to the measurable charge polarization susceptibility. The generalization to nonzero temperature is an important milestone to address topology in more realistic scenarios.

We now discuss a numerical protocol to evaluate the nonzero temperature Chern marker spectral functions. In terms of the eigenstate projector  $S_\ell = |E_\ell\rangle\langle E_\ell|$  and  $f_{\ell\ell'} \equiv f(E_\ell) - f(E_{\ell'})$ , the spectral function in Eq. (22) summing over all lattice sites can be rewritten as

$$\begin{aligned} \mathcal{C}^d(\omega) &= \sum_{\mathbf{r}} \mathcal{C}^d(\mathbf{r}, \omega) \\ &= \text{Tr} \sum_{\ell < \ell'} [i X_{\ell\ell'} Y_{\ell'\ell} f_{\ell\ell'} \delta(\omega + E_\ell - E_{\ell'}) - (x \leftrightarrow y)], \end{aligned} \quad (24)$$

where  $X_{\ell\ell'} \equiv S_\ell \hat{x} S_{\ell'}$  and  $Y_{\ell'\ell} \equiv S_{\ell'} \hat{y} S_\ell$ . We first evaluate the matrix

$$X(\omega) = \sum_{\ell < \ell'} S_\ell \hat{x} S_{\ell'} \sqrt{f_{\ell\ell'} \delta(\omega + E_\ell - E_{\ell'})}, \quad (25)$$

and the analogous  $Y(\omega)$  given by replacing  $\hat{x} \rightarrow \hat{y}$ . To implement the square root, we use an approximation of the delta function as a Lorentzian of breadth  $\eta$ , i.e.

$\delta(x) = \eta/\pi(x^2 + \eta^2)$ . Expressed in terms of these matrices, the Chern marker spectral function is simply

$$\mathcal{C}^d(\mathbf{r}, \omega) = i\langle \mathbf{r} | [X(\omega)Y^\dagger(\omega) - Y(\omega)X^\dagger(\omega)] | \mathbf{r} \rangle. \quad (26)$$

Alternatively, the Chern marker (and hence the Chern number) can be directly evaluated by computing the frequency independent matrices

$$X = \sum_{\ell < \ell'} S_\ell \hat{x} S_{\ell'} \sqrt{f_{\ell\ell'}}, \quad (27)$$

and likewise  $Y$ , such that

$$\mathcal{C}^d(\mathbf{r}) = i\langle \mathbf{r} | [X Y^\dagger - Y X^\dagger] | \mathbf{r} \rangle. \quad (28)$$

### 3. Lattice model of Chern insulator

We now illustrate the power of the concepts described in the previous sections to the concrete example of a prototypical 2D Chern insulator. The two band lattice Hamiltonian is [33]

$$\begin{aligned} H = & \sum_i t \left\{ -i c_{is}^\dagger c_{i+ap} + i c_{i+as}^\dagger c_{ip} - c_{is}^\dagger c_{i+bp} + c_{i+bs}^\dagger c_{ip} + h.c. \right\} \\ & + \sum_{i\delta} t' \left\{ -c_{is}^\dagger c_{i+\delta s} + c_{ip}^\dagger c_{i+\delta p} + h.c. \right\} \\ & + \sum_i (M + 4t') \left\{ c_{is}^\dagger c_{is} - c_{ip}^\dagger c_{ip} \right\}, \end{aligned} \quad (29)$$

where  $\delta = \{a, b\}$  represents the shift to the neighbouring sites in the two planar directions. The internal degrees of freedom  $\sigma = \{s, p\}$  are the orbitals. The corresponding momentum space Hamiltonian in the basis  $(c_{\mathbf{k}s}, c_{\mathbf{k}p})^T$  is given by [34, 35]

$$\begin{aligned} H(\mathbf{k}) = & 2t \sin k_x \sigma^x + 2t \sin k_y \sigma^y \\ & + (M + 4t' - 2t' \cos k_x - 2t' \cos k_y) \sigma^z. \end{aligned} \quad (30)$$

Throughout the paper, we set  $t = t' = 1.0$  and tune the mass term  $M$  and temperature  $k_B T$  to examine different topological phases. The model has topological phase transitions (TPT) at three critical points  $M_c = \{-8, -4, 0\}$ , reflecting gap closures at different high symmetry points (HSPs) in momentum space [36]. Since they all exhibit the same critical behavior [25, 26, 27], we will focus on the  $M_c = 0$  critical point where the bulk gap closes at  $\mathbf{k} = (0, 0)$ .

Analytical results for this model can be obtained by linearizing the Hamiltonian near the HSP  $\mathbf{k}_0 = (0, 0)$ , yielding  $E_{m,n} = \pm \sqrt{M^2 + v^2 k^2}$  and a zero temperature Berry curvature  $\Omega_{xy} = v^2 M / 2 (M^2 + v^2 k^2)^{3/2}$ . The Chern number and Chern marker spectral functions are equivalent in this homogeneous model, giving (restoring  $\hbar$ )

$$\begin{aligned} \mathcal{C}^d(\omega) = & \int \frac{d^2 \mathbf{k}}{(2\pi)^2} \Omega_{xy} [f(E_n) - f(E_m)] \delta(\omega + E_n/\hbar - E_m/\hbar) \\ = & \frac{M}{2\pi \hbar \omega^2} \left[ f\left(-\frac{\hbar \omega}{2}\right) - f\left(\frac{\hbar \omega}{2}\right) \right]_{\omega \geq 2|M|/\hbar}. \end{aligned} \quad (31)$$

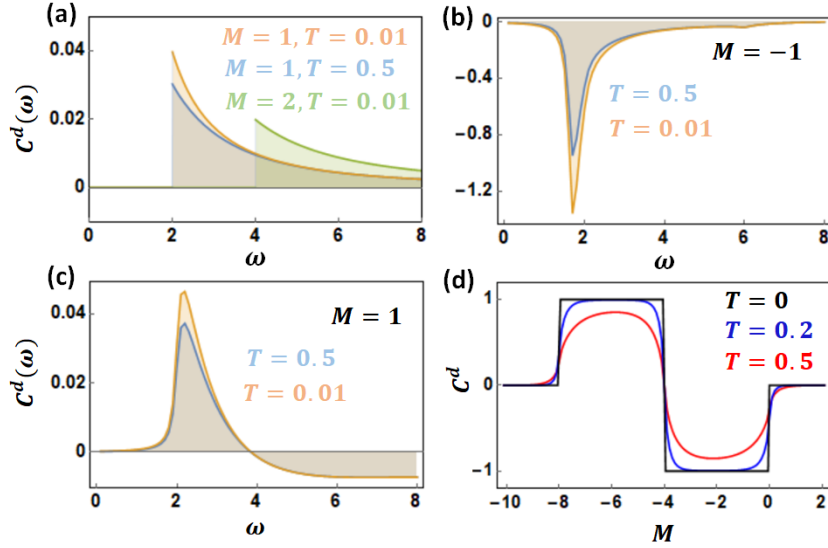


**Figure 1.** (a) The Chern number/marker spectral function  $C^d(\omega)$  for the Chern insulator in a continuum, which is finite only at frequency larger than the bulk gap  $M$ , and moreover scales like  $1/\omega^2$  such that it integrates to a topological invariant. The overall magnitude is reduced at nonzero temperature. (b) The  $C^d(\omega)$  for the lattice model of Chern insulator in the topologically nontrivial phase  $M = -1$ , where the  $\delta$ -function in Eq. (31) is simulated by a Lorentzian with width  $\eta = 0.1$ . The spectral function is negative due to the negative Chern number  $C^d \approx -1$ . (c) The  $C^d(\omega)$  for the lattice model in the topologically nontrivial phase  $M = 1$ , whose positive and negative regions together yield  $C^d \approx 0$  (up to numerical precision). (d) The frequency-integrated Chern number/marker  $C^d$  at zero and nonzero temperatures as a function of the mass term  $M$ .

At zero temperature  $C^d(\omega) \rightarrow \mathcal{C}(\omega)$ , the spectral function is nonzero only if  $\omega \geq 2|M|/\hbar$  as expected, since it represents an exciton absorption rate, as shown schematically in Fig. 1 (a). Moreover, the spectral function scales like  $1/\omega^2$ , such that it integrates to a constant topological invariant  $\mathcal{C} = \int_{2|M|/\hbar}^{\infty} d\omega \mathcal{C}(\omega) = \text{Sgn}(M)/4\pi$ . Essentially, this is the  $f$ -sum rule of exciton absorption rate in circular dichroism applied to topological insulators [32]. At nonzero temperature, since the Fermi factor  $f(-\frac{\omega}{2}) - f(\frac{\omega}{2}) \leq 1$ ,  $C^d < \text{Sgn}(M)/4\pi$  smaller than the true topological invariant, as illustrated in Fig. 1 (a). We anticipate that these predicted features should be readily verifiable by the experiments proposed in Secs. 2.2 and 2.3.

The numerical results of  $C^d(\mathbf{r}, \omega) = C^d(\omega)$  for the homogeneous lattice model of Chern insulator in Eq. (30) are shown in Fig. 1 (b) for the topologically nontrivial phase  $M = -1$ . The spectral function is negative (consistent with  $C = -1$ ) and the magnitude is largest near the band gap  $2|M| = 2$ , reflecting that excitations of states in the vicinity of the band gap are the most detrimental to the topological properties of the system. In the topologically trivial phase  $M = 1$  shown in Fig. 1 (c), the spectral weight has both positive and negative components such that it integrates to a zero Chern number  $C^d \approx 0$ . Comparing Fig. 1 (b) and (c), we see that the spectral weight near the band



gap flips sign as the system crosses the TPT at  $M = 0$ , in accordance with the flipping of Berry curvature at the HSP  $\mathbf{k}_0 = (0, 0)$ , a defining feature of TPTs [37, 25, 26, 27]. This is also true at the other TPTs at  $M = \{-8, -4\}$  at which  $\mathcal{C}$  changes abruptly. To summarize, we see that though abrupt changes of the Chern number at the critical points are smeared out at nonzero temperature as shown in Fig. 1 (d), clear vestiges of these TPTs are present in the Chern markers and spectral functions and should be observable in the experimentally accessible temperature range.

#### 4. Topological quantum criticality

The Chern marker is known to display interesting critical behavior near TPTs, such as size-dependent smoothening of its discontinuity [38], Kibble-Zurek scaling in disordered Chern insulators [39], and Hofstadter-butterfly-like features in quasicrystals [40], which may be investigated in Chern insulators constructed from amorphous random points [41] or ultracold dysprosium atoms with a synthetic dimension [42]. As with standard symmetry breaking critical points, where correlation functions of the order parameter show divergent correlation lengths, we explore if there exist certain nonlocal correlators that will display such singular behavior near TPTs. In this section, we use the linear response theory of the Chern marker outlined above to identify two quantities: a *Chern correlator* and a *nonlocal Chern marker*, which encode different physics pertaining to criticality and topological correlation.

##### 4.1. Chern correlator as a nonlocal charge polarization susceptibility

We consider first the zero temperature limit. Following Eqs. (12), (13) and (20), we define the nonlocal Chern correlator

$$\begin{aligned} \tilde{\mathcal{C}}(\mathbf{r}, \mathbf{r}') &= \text{Re} \langle \mathbf{r} | \left[ i\hat{P}\hat{x}\hat{Q}\hat{y}_{\mathbf{r}'} - i\hat{P}\hat{y}\hat{Q}\hat{x}_{\mathbf{r}'} \right] | \mathbf{r} \rangle \\ &= \sum_{nm} \text{Re} \{ i \langle E_n | \hat{x}_{\mathbf{r}} | E_m \rangle \langle E_m | \hat{y}_{\mathbf{r}'} | E_n \rangle - (x \leftrightarrow y) \}, \end{aligned} \quad (32)$$

which sums to the Chern marker  $\sum_{\mathbf{r}'} \tilde{\mathcal{C}}(\mathbf{r}, \mathbf{r}') = \mathcal{C}(\mathbf{r})$ . This Chern correlator represents a measure of topological correlation in the system. For instance, in a clean and infinite system at zero temperature, the local Chern marker  $\mathcal{C}(\mathbf{r}) = \mathcal{C}$  is a constant for all  $\mathbf{r}$ , and this remains true even when the system approaches a TPT. However, the Chern correlator  $\tilde{\mathcal{C}}(\mathbf{r}, \mathbf{r}')$  as a function of  $\mathbf{r} - \mathbf{r}'$  changes its profile as the system enters a topologically nontrivial phase, and can therefore act as a proxy for the amount of spatial topological correlation in the system.

To demonstrate this feature, numerical results for the Chern insulator in the lattice model are shown in Fig. 2. Typically, the correlations are maximal deep in a topological phase and very weak in topologically trivial phases. The Chern correlator consists mainly of two peaks of opposite sign around  $\mathbf{r} \sim \mathbf{r}'$  consistent with the expectation that nonlocal charge polarization susceptibilities are larger at short separations. A pronounced asymmetry between the heights of the two peaks is seen in topologically

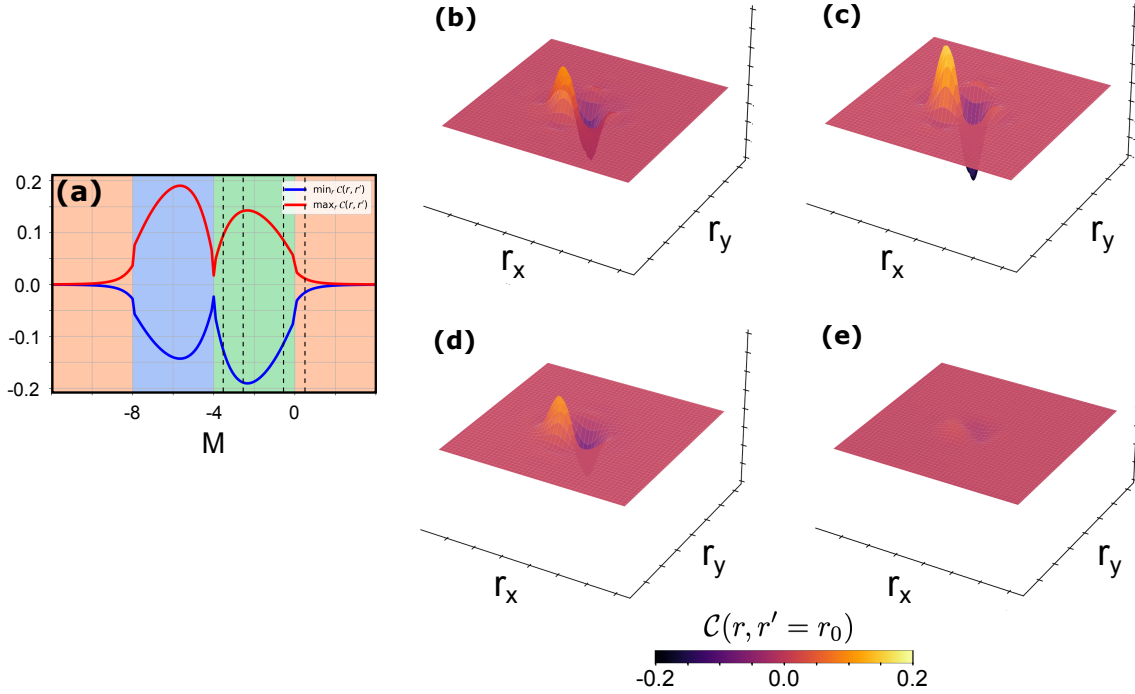


**Figure 2.** (a) The maximal and minimal values of the zero-temperature Chern correlator  $\tilde{C}(\mathbf{r}, \mathbf{r}')$  as a function of the tuning parameter  $M$  for a Chern insulator on a  $14 \times 14$  lattice. The background color indicates the three topologically distinct phases. The vertical dashed lines indicate the surface plots of  $\tilde{C}(\mathbf{r}, \mathbf{r}' = \mathbf{r}_0)$  with  $r_0 = (7, 7)$ , shown in the right panels: (b)  $M = -3.5$ , (c)  $M = -2.5$ , (d)  $M = -0.5$ , (e)  $M = 0.5$ . The surface plots have been interpolated on a  $140 \times 140$  grid as a visual aid.

non trivial phases whereas the peak heights are equal in the topologically trivial phase, concomitant with the expectation that the spatial integral of this correlator should yield the Chern number. These aspects are well encapsulated in Fig. 2(a) where we see the evolution of the two peak heights as a function of  $M$ . These features suggest that the nonlocal charge polarization susceptibility indeed presents a physical measure of topological correlations in a system.

The nonzero temperature version of the Chern correlator can be constructed by means of our linear response formalism for the circular dichroism, leading us to consider

$$\tilde{C}^d(\mathbf{r}, \mathbf{r}', \omega) = -\frac{1}{\pi} \text{Re} [\chi_{xy}(\mathbf{r}, \mathbf{r}', \omega) - \chi_{yx}(\mathbf{r}, \mathbf{r}', \omega)]. \quad (33)$$

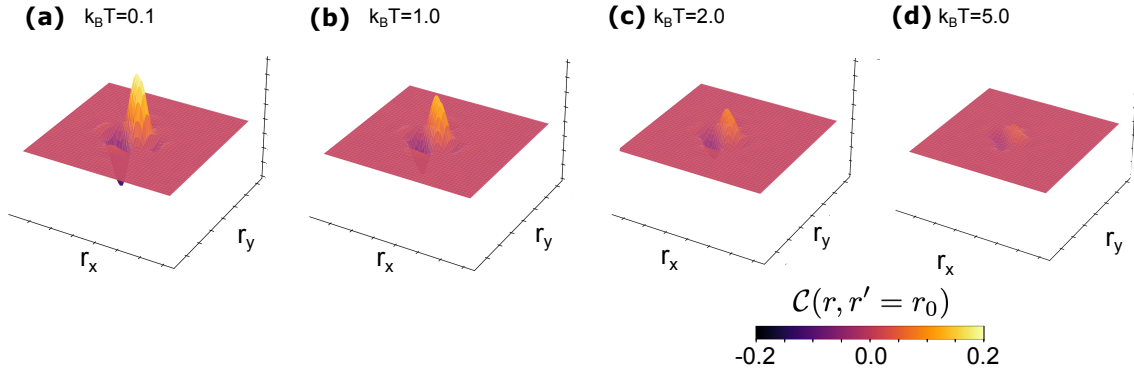
The Chern correlator is then  $\tilde{C}^d(\mathbf{r}, \mathbf{r}') = \int d\omega \tilde{C}^d(\mathbf{r}, \mathbf{r}', \omega)$ . Using the numerical protocol discussed in Sec. 2.3, we can show that

$$\begin{aligned} \tilde{C}^d(\mathbf{r}, \mathbf{r}', \omega) &= i \langle \mathbf{r} | \left[ X(\omega) Y_{\mathbf{r}'}^\dagger(\omega) - Y(\omega) X_{\mathbf{r}'}^\dagger(\omega) \right] | \mathbf{r} \rangle, \\ \tilde{C}^d(\mathbf{r}, \mathbf{r}') &= i \langle \mathbf{r} | \left[ X Y_{\mathbf{r}'}^\dagger - Y X_{\mathbf{r}'}^\dagger \right] | \mathbf{r} \rangle \end{aligned} \quad (34)$$

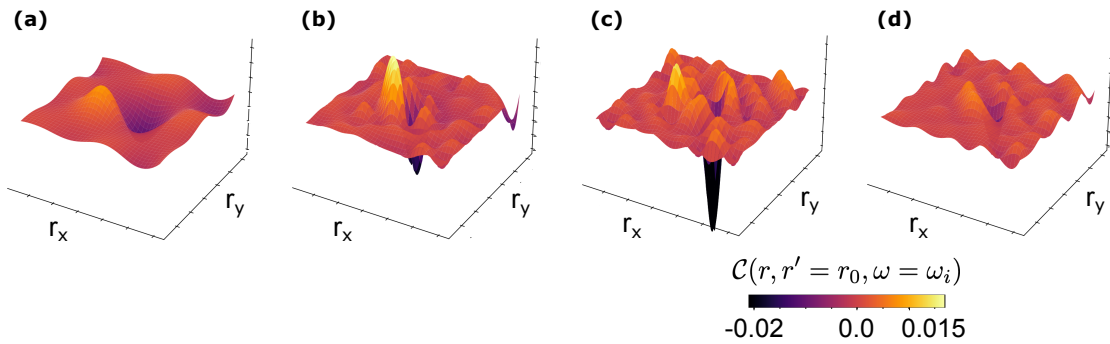
where  $X, Y$  are defined in Eqs. (25) and (27).

Fig. 3 shows the temperature evolution of Chern correlator  $\tilde{C}^d(\mathbf{r}, \mathbf{r}')$  in the topologically nontrivial phase at  $M = -5.5$ . For  $T \ll 2|M|$  (panel (a)), the

correlator remains essentially unchanged from the zero-temperature case shown in Fig. 2. Qualitative features like the height asymmetry of the peaks in the topologically nontrivial phases remain unaltered. For larger temperatures, (panels (b)-(d)), the Chern correlator becomes progressively weaker, in accordance with the reduction of the Chern marker from its zero-temperature value shown in Fig. 1 (d). The frequency dependent Chern correlator  $\tilde{\mathcal{C}}^d(\mathbf{r}, \mathbf{r}', \omega)$  is shown in Fig. 4. Note that the spectral function exhibits a rich spatial structure, indicating that the correlation within the system can vary a lot depending on the probed frequency.



**Figure 3.** The nonzero temperature Chern correlator for a Chern insulator on a  $14 \times 14$  lattice at  $M = -5.5$ . The reference point is  $r_0 = (7, 7)$ . The panels show four increasing values of the temperature  $k_B T$ : (a)  $k_B T = 0.1$ , (b)  $k_B T = 0.5$ , (c)  $k_B T = 2.0$ , (d)  $k_B T = 5.0$ . The other parameters are  $t = t' = B = 1.0$  and  $\mu = 0.0$  for all panels. The surface plots have been interpolated on a  $140 \times 140$  grid as a visual aid.



**Figure 4.** Chern correlator spectral function  $\tilde{\mathcal{C}}(\mathbf{r}, \mathbf{r}' = r_0, \omega = \omega_i)$  at various values of the frequency  $\omega_i$  for a Chern insulator at  $M = -1.0$  and temperature  $k_B T = 0.1$  on a  $12 \times 12$  lattice. The reference point is  $r_0 = (6, 6)$ . (a)  $\omega_i = 2.7$ , (b)  $\omega_i = 5.6$ , (c)  $\omega_i = 5.9$ , (d)  $\omega_i = 6.9$ . In the numerics, the delta function was approximated by a Lorentzian with width parameter  $\eta = 0.1$ . The surface plots have been interpolated on a  $120 \times 120$  grid as a visual aid.

#### 4.2. Wannier state correlation function as a nonlocal Chern marker

Lastly, we highlight the intricate link between Chern markers and a previously proposed Wannier state correlation function [25, 26, 27], Restricting ourselves to a homogeneous system at zero temperature, the Wannier state correlation function derived from the Fourier transform of the Berry curvature  $\Omega_{xy}$  is [30, 31, 43]

$$\begin{aligned}\tilde{F}(\mathbf{R}) &= \int \frac{d^2\mathbf{k}}{(2\pi)^2} \Omega_{xy}(\mathbf{k}) e^{i\mathbf{k}\cdot\mathbf{R}} = -i \sum_n \langle \mathbf{R}n | (R_x \hat{y} - R_y \hat{x}) | \mathbf{0}n \rangle \\ &= -i \sum_n \int d^2\mathbf{r} (R_x y - R_y x) W_n(\mathbf{r} - \mathbf{R})^* W_n(\mathbf{r})\end{aligned}\quad (35)$$

provided  $\mathbf{R} \neq \mathbf{0}$ . The Lorentzian shape of the Berry curvature  $\Omega_{xy}(\mathbf{k})$  with width  $\xi^{-1}$  results in a decaying  $\tilde{F}(\mathbf{R})$  with correlation length  $\xi$ . As the system approaches the TPTs,  $\xi \rightarrow \infty$ . This is a generic feature of TPTs both in and out of equilibrium [44, 45], from which the critical exponent of  $\xi$  can be extracted [25, 26, 27]. We remark that the spatial profile of  $\tilde{F}(\mathbf{R})$  for the lattice Chern insulator of Eq. (29) has already been shown in Fig. 3 of Ref. [25].

On the other hand, using the formalism in Sec. 2.1, we can see that

$$\begin{aligned}\tilde{F}(\mathbf{R}) &= \sum_n \int \frac{d^2\mathbf{k}}{(2\pi)^2} i \langle \partial_x u_{n\mathbf{k}} | \partial_y u_{n\mathbf{k}} \rangle e^{i\mathbf{k}\cdot\mathbf{R}} - (x \leftrightarrow y) \\ &= \sum_n \sum_m \int \frac{d^2\mathbf{k}}{(2\pi)^2} \int \frac{d^2\mathbf{k}'}{(2\pi)^2} i \langle \psi_{n\mathbf{k}} | \hat{x} | \psi_{m\mathbf{k}'} \rangle \langle \psi_{m\mathbf{k}'} | \hat{y} | \psi_{n\mathbf{k}} \rangle e^{i\mathbf{k}\cdot\mathbf{R}} \\ &\quad - (x \leftrightarrow y).\end{aligned}\quad (36)$$

Since  $\mathbf{R}$  is a Bravais lattice vector and  $u_{n\mathbf{k}}(\mathbf{r}) = u_{n\mathbf{k}}(\mathbf{r} + \mathbf{R})$  is cell periodic,

$$\langle \mathbf{r} | \psi_{n\mathbf{k}} \rangle e^{i\mathbf{k}\cdot\mathbf{R}} = e^{i\mathbf{k}\cdot(\mathbf{r}+\mathbf{R})} u_{n\mathbf{k}}(\mathbf{r} + \mathbf{R}) = \psi_{n\mathbf{k}}(\mathbf{r} + \mathbf{R}) = \langle \mathbf{r} + \mathbf{R} | \psi_{n\mathbf{k}} \rangle. \quad (37)$$

In other words,  $|\psi_{n\mathbf{k}}\rangle e^{i\mathbf{k}\cdot\mathbf{R}}$  projected to  $\langle \mathbf{r} |$  is equivalent to  $|\psi_{n\mathbf{k}}\rangle$  projected to  $\langle \mathbf{r} + \mathbf{R} |$ . In parallel, using the projector operator formalism, we can define a nonlocal Chern marker  $\mathcal{C}(\mathbf{r} + \mathbf{R}, \mathbf{r})$  from the off-diagonal element of the Chern operator

$$\mathcal{C}(\mathbf{r} + \mathbf{R}, \mathbf{r}) \equiv i \langle \mathbf{r} + \mathbf{R} | \left[ \hat{P} \hat{x} \hat{Q} \hat{y} - \hat{P} \hat{y} \hat{Q} \hat{x} \right] | \mathbf{r} \rangle. \quad (38)$$

Note that the case  $\mathbf{R} = 0$  reduces to the standard Chern marker  $\mathcal{C}(\mathbf{r})$ . Using Eq. (37), one sees that for homogeneous systems, the nonlocal Chern marker is precisely the Wannier state correlation function

$$\lim_{N \rightarrow \infty} \text{Re} [\mathcal{C}(\mathbf{r} + \mathbf{R}, \mathbf{r})] = \tilde{F}(\mathbf{R}), \quad (39)$$

where we take the real part at the end because  $\tilde{F}(\mathbf{R})$  is real in practice, since the Berry curvature is a real quantity. As  $\mathcal{C}(\mathbf{r} + \mathbf{R}, \mathbf{r})$  involves off-diagonal elements  $\langle \mathbf{r} + \mathbf{R} | \dots | \mathbf{r} \rangle$  of the Chern operator, it does not have a straightforward interpretation within linear response theory.

The spatial profile of  $\mathcal{C}(\mathbf{r} + \mathbf{R}, \mathbf{r})$  for the lattice Chern insulator in Eq. (29) is shown in Fig. 5, where we choose  $\mathbf{r}$  to be the center of the lattice and plot it as a function

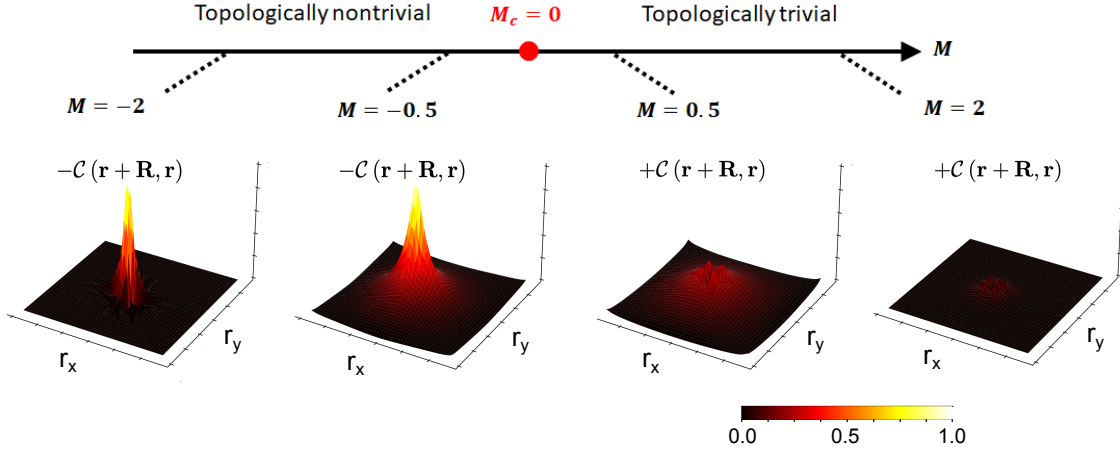


**Figure 5.** The nonlocal Chern marker  $\mathcal{C}(\mathbf{r} + \mathbf{R}, \mathbf{r})$  of the lattice Chern insulator of size  $28 \times 28$  sites, where we choose  $\mathbf{r}$  to be at the center of the lattice and plot it as a function of  $\mathbf{R}$  for four values of  $M$ . One sees that the spatial profiles closer to the critical point  $M = \pm 0.5$  are more long-ranged than those far away from the critical point  $M = \pm 2$ . Note that we plot  $-\mathcal{C}(\mathbf{r} + \mathbf{R}, \mathbf{r})$  for the topologically nontrivial phase since the Chern marker  $\mathcal{C}(r) \approx -1$  gives an overall negative amplitude.

of  $\mathbf{R}$  for parameters close and far away from the critical point  $M_c = 0$ . As expected,  $\mathcal{C}(\mathbf{r} + \mathbf{0}, \mathbf{r}) = \mathcal{C}(\mathbf{r}) \approx 0$  or  $-1$  in the two distinct topological phases and  $\mathcal{C}(\mathbf{r} + \mathbf{R}, \mathbf{r})$  decreases with  $\mathbf{R}$ . Due to the diverging correlation length  $\xi$ ,  $\mathcal{C}(\mathbf{r} + \mathbf{R}, \mathbf{r})$  becomes more long-ranged as the system approaches the critical point  $M_c = 0$  from either side of the transition, thereby serving as a faithful measure to the critical behavior near TPTs. We remark that the critical exponent of the correlation length  $\xi \sim |M|^{-\nu}$  has been calculated previously from the divergence of Berry curvature, yielding  $\nu = 1$  for linear Dirac models [25, 46, 27, 26, 45, 44].

## 5. Conclusions

In summary, we extend the theory of local Chern markers  $\mathcal{C}(\mathbf{r})$  at zero temperature to introduce various new aspects about the topological order, topological correlation, and topological quantum criticality in real space. The first is the Chern correlator  $\tilde{\mathcal{C}}(\mathbf{r}, \mathbf{r}')$  that is sensitive to both the value of the Chern marker in each topological phase, and presents a measure of topological correlations of the system. These correlations increase as the system enter a topologically nontrivial phase, reaching a maximum deep inside the phase. In addition, we introduce a nonlocal Chern marker  $\mathcal{C}(\mathbf{r} + \mathbf{R}, \mathbf{r})$  obtained from the off-diagonal element of the Chern operator. We demonstrate that it corresponds to a previously proposed Wannier state correlation function. As the system approaches TPTs, the divergence of Berry curvature at the gap-closing momentum causes the nonlocal Chern marker to become increasingly longer-ranged, and thus it serves as tool to investigate topological quantum criticality.

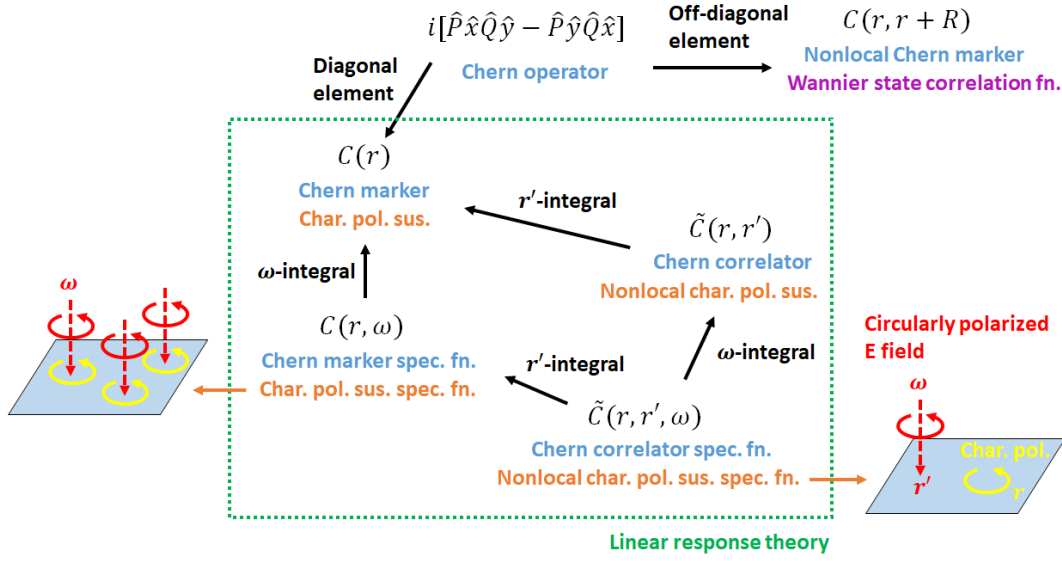


**Figure 6.** Summary of the linear response theory, measurement protocols, and Wannier function interpretation of various quantities introduced in the present work. The blue text gives the terminology, the orange text the corresponding physical quantity in the proposed circular dichroism experiment shown in the two figures, and the black arrows the relation between them. The abbreviations are char.= charge, pol.= polarization, sus.= susceptibility, spec. = spectral, and fn. = function.

We then present a linear response theory to generalize these real space markers to nonzero temperature, and show that these real space measures are intimately linked to experimentally measurable quantities. The generalized local Chern marker  $\mathcal{C}^d(\mathbf{r})$  is related to the charge polarization caused by a circularly polarized electric field. The corresponding Chern marker spectral function  $\mathcal{C}^d(\mathbf{r}, \omega)$  encapsulates the local absorption rate at  $\mathbf{r}$  caused by a circularly polarized oscillatory electric field of frequency  $\omega$ , which is predicted to scale as  $\sim 1/\omega^2$  for frequencies near the band gap. Similarly, the Chern correlator spectral function  $\mathcal{C}^d(\mathbf{r}, \mathbf{r}', \omega)$  is the nonlocal charge polarization at  $\mathbf{r}$  caused by an oscillatory field localized around  $\mathbf{r}'$ , whose spatial profile strongly depends on the frequency  $\omega$ .

All of these quantities can be measured in appropriately tailored circular dichroism experiments. We emphasize that these measures are not restricted to the Chern insulator presented in this work, but can be used to investigate topological order and topological quantum criticality in a wide class of 2D TR breaking materials. In particular, our theory may help to address the influence of spatial inhomogeneity such as disorder and grain boundaries in a realistic nonzero temperature setup, allowing the experimental measurable local and nonlocal spectral functions to be calculated. All these broad range of applications await to be further investigated.

## 6. Acknowledgments

This work is partially supported by the ESPRC Grant no. EP/P009565/1. W. C. acknowledges the financial support of the productivity in research fellowship from CNPq. We also acknowledge computation time on the ETH Euler cluster.

- [1] F. D. M. Haldane. Model for a quantum hall effect without landau levels: Condensed-matter realization of the "parity anomaly". *Phys. Rev. Lett.*, 61:2015–2018, October 1988.
- [2] D. J. Thouless, M. Kohmoto, M. P. Nightingale, and M. den Nijs. Quantized hall conductance in a two-dimensional periodic potential. *Phys. Rev. Lett.*, 49:405–408, August 1982.
- [3] J. Bellissard, A. van Elst, and H. Schulz-Baldes. The noncommutative geometry of the quantum hall effect. *J. Math. Phys.*, 35(10):5373–5451, 1994.
- [4] Emil Prodan, Taylor L. Hughes, and B. Andrei Bernevig. Entanglement spectrum of a disordered topological chern insulator. *Phys. Rev. Lett.*, 105:115501, Sep 2010.
- [5] Emil Prodan. Non-commutative tools for topological insulators. *New J. Phys.*, 12(6):065003, jun 2010.
- [6] Emil Prodan. Disordered topological insulators: a non-commutative geometry perspective. *J. Phys. A: Math. Theor.*, 44(11):113001, feb 2011.
- [7] Raffaello Bianco and Raffaele Resta. Mapping topological order in coordinate space. *Phys. Rev. B*, 84:241106, December 2011.
- [8] Raffaello Bianco and Raffaele Resta. Orbital magnetization as a local property. *Phys. Rev. Lett.*, 110:087202, Feb 2013.
- [9] Antimo Marrazzo and Raffaele Resta. Locality of the anomalous hall conductivity. *Phys. Rev. B*, 95:121114, Mar 2017.
- [10] Alexei Kitaev. Anyons in an exactly solved model and beyond. *Ann. Phys.*, 321(1):2–111, 2006. January Special Issue.
- [11] Yi-Fu Zhang, Yun-You Yang, Yan Ju, Li Sheng, Rui Shen, Dong-Ning Sheng, and Ding-Yu Xing. Coupling-matrix approach to the chern number calculation in disordered systems. *Chin. Phys. B*, 22(11):117312, nov 2013.
- [12] D. Carvalho, N. A. García-Martínez, J. L. Lado, and J. Fernández-Rossier. Real-space mapping of topological invariants using artificial neural networks. *Phys. Rev. B*, 97:115453, Mar 2018.
- [13] T. A. Loring and M. B. Hastings. Disordered topological insulators via  $c^*$ -algebras. *EPL*, 92(6):67004, dec 2010.
- [14] Ian Mondragon-Shem, Taylor L. Hughes, Juntao Song, and Emil Prodan. Topological criticality in the chiral-symmetric aiii class at strong disorder. *Phys. Rev. Lett.*, 113:046802, Jul 2014.
- [15] Huaqing Huang and Feng Liu. Quantum spin hall effect and spin bott index in a quasicrystal lattice. *Phys. Rev. Lett.*, 121:126401, Sep 2018.
- [16] Juntao Song and Emil Prodan. Aiii and bdi topological systems at strong disorder. *Phys. Rev. B*, 89:224203, Jun 2014.
- [17] Juntao Song, Carolyn Fine, and Emil Prodan. Effect of strong disorder on three-dimensional chiral topological insulators: Phase diagrams, maps of the bulk invariant, and existence of topological extended bulk states. *Phys. Rev. B*, 90:184201, Nov 2014.
- [18] Fei Song, Shunyu Yao, and Zhong Wang. Non-hermitian topological invariants in real space. *Phys. Rev. Lett.*, 123:246801, Dec 2019.
- [19] Duc Thanh Tran, Alexandre Dauphin, Adolfo G. Grushin, Peter Zoller, and Nathan Goldman. Probing topology by heating: Quantized circular dichroism in ultracold atoms. *Sci. Adv.*, 3(8):e1701207, 2017.
- [20] Luca Asteria, Duc Thanh Tran, Tomoki Ozawa, Matthias Tarnowski, Benno S. Rem, Nick Fläschner, Klaus Sengstock, Nathan Goldman, and Christof Weitenberg. Measuring quantized

- circular dichroism in ultracold topological matter. *Nat. Phys.*, 15:449, 2019.
- [21] Quentin Marsal, Dániel Varjas, and Adolfo G. Grushin. Topological weaire–thorpe models of amorphous matter. *Proceedings of the National Academy of Sciences*, 117(48):30260–30265, 2020.
- [22] Philipp W. Klein, Adolfo G. Grushin, and Karyn Le Hur. Interacting stochastic topology and mott transition from light response. *Phys. Rev. B*, 103:035114, 2021.
- [23] C. Repellin and N. Goldman. Detecting fractional chern insulators through circular dichroism. *Phys. Rev. Lett.*, 122:166801, Apr 2019.
- [24] Wei Chen and Gero von Gersdorff. Measurement of interaction-dressed berry curvature and quantum metric in solids by optical absorption. *arXiv:2202.03494*, 2022.
- [25] Wei Chen, Markus Legner, Andreas Rüegg, and Manfred Sigrist. Correlation length, universality classes, and scaling laws associated with topological phase transitions. *Phys. Rev. B*, 95:075116, Feb 2017.
- [26] Wei Chen and Manfred Sigrist. *Advanced Topological Insulators, Ch. 7*. Wiley-Scrivener, March 2019.
- [27] Wei Chen and Andreas P Schnyder. Universality classes of topological phase transitions with higher-order band crossing. *New J. Phys.*, 21(7):073003, jul 2019.
- [28] Gero von Gersdorff and Wei Chen. Measurement of topological order based on metric-curvature correspondence. *Phys. Rev. B*, 104:195133, Nov 2021.
- [29] Nicola Marzari and David Vanderbilt. Maximally localized generalized wannier functions for composite energy bands. *Phys. Rev. B*, 56:12847–12865, November 1997.
- [30] Nicola Marzari, Arash A. Mostofi, Jonathan R. Yates, Ivo Souza, and David Vanderbilt. Maximally localized wannier functions: Theory and applications. *Rev. Mod. Phys.*, 84:1419–1475, October 2012.
- [31] M. Gradhand, D. V. Fedorov, F. Pientka, P. Zahn, I. Mertig, and B. L. Györfy. First-principle calculations of the berry curvature of bloch states for charge and spin transport of electrons. *J. Phys. Condens. Matter*, 24(21):213202, 2012.
- [32] Ivo Souza and David Vanderbilt. Dichroic  $f$ -sum rule and the orbital magnetization of crystals. *Phys. Rev. B*, 77:054438, February 2008.
- [33] Wei Chen. Absence of equilibrium edge currents in theoretical models of topological insulators. *Phys. Rev. B*, 101:195120, May 2020.
- [34] Xiao-Liang Qi and Shou-Cheng Zhang. Topological insulators and superconductors. *Rev. Mod. Phys.*, 83:1057–1110, October 2011.
- [35] B. Andrei Bernevig and Taylor L. Hughes. *Topological Insulators and Topological Superconductors*. Princeton University Press, April 2013.
- [36] Paolo Molignini, Antonio Zegarra, Evert van Nieuwenburg, R. Chitra, and Wei Chen. A supervised learning algorithm for interacting topological insulators based on local curvature. *SciPost Phys.*, 11:073, 2021.
- [37] Wei Chen. Scaling theory of topological phase transitions. *J. Phys. Condens. Matter*, 28(5):055601, 2016.
- [38] M. D. Caio, G. Möller, N. R. Cooper, and M. J. Bhaseen. Topological marker currents in chern insulators. *Nat. Phys.*, 15(3):257–261, Mar 2019.
- [39] Lara Ulčakar, Jernej Mravlje, and Tomaž Rejec. Kibble-zurek behavior in disordered chern insulators. *Phys. Rev. Lett.*, 125:216601, Nov 2020.
- [40] Duc-Thanh Tran, Alexandre Dauphin, Nathan Goldman, and Pierre Gaspard. Topological hofstadter insulators in a two-dimensional quasicrystal. *Phys. Rev. B*, 91:085125, Feb 2015.
- [41] Noah P. Mitchell, Lisa M. Nash, Daniel Hexner, Ari M. Turner, and William T. M. Irvine. Amorphous topological insulators constructed from random point sets. *Nat. Phys.*, 14(4):380–385, Apr 2018.
- [42] Thomas Chalopin, Tanish Satoor, Alexandre Evrard, Vasilij Makhlov, Jean Dalibard, Raphael Lopes, and Sylvain Nascimbene. Probing chiral edge dynamics and bulk topology of a synthetic



- hall system. *Nat. Phys.*, 16(10):1017–1021, Oct 2020.
- [43] Xinjie Wang, Jonathan R. Yates, Ivo Souza, and David Vanderbilt. *Ab initio* calculation of the anomalous hall conductivity by wannier interpolation. *Phys. Rev. B*, 74:195118, November 2006.
- [44] Paolo Molignini, Wei Chen, and R. Chitra. Generating quantum multicriticality in topological insulators by periodic driving. *Phys. Rev. B*, 101:165106, Apr 2020.
- [45] P. Molignini, W. Chen, and R. Chitra. Unifying topological phase transitions in noninteracting, interacting, and periodically driven systems. *Europhys. Lett.*, 128:36001, 2019.
- [46] Paolo Molignini, Wei Chen, and R. Chitra. Universal quantum criticality in static and floquet-majorana chains. *Phys. Rev. B*, 98:125129, Sep 2018.